Processing and Application of Ceramics 13 [4] (2019) 411–417
https://doi.org/10.2298/PAC1904411L

Impact of calcium doping on structure, catalytic and conductive properties of lanthanum strontium iron oxide

Łukasz Łańcucki, Radosław Lach, Paweł Nieroda, Ewa Drożdż, Paweł Pasierb*

AGH University of Science and Technology, Faculty of Materials Science and Ceramics, al. A Mickiewicza 30, 30-059 Kraków, Poland

Received 7 January 2019; Received in revised form 9 May 2019; Received in revised form 4 September 2019; Accepted 20 November 2019

Abstract

A set of dense structure materials based on $La_{0.5}Sr_{0.5-x}Ca_xFeO_3$ with different amount of calcium (where x varies from 0 to 0.1) were prepared. It was found that with calcium addition the hexagonal perovskite $La_{0.5}Sr_{0.5}FeO_3$ structure is preserved and Ca^{2+} ions accommodate themselves easily in the lattice. The sintered ceramics have homogeneous microstructure and uniform grain size distribution with the average size which increases with Ca addition. Electrical properties of the sintered materials determined by the DC method revealed an increase in sample conductivity with Ca^{2+} doping. An increase in structure stability with the increase of calcium addition was also confirmed by the temperature-programmed studies.

Keywords: *lanthanum iron oxide, perovskites, citrate method, catalytic activity, electrical conductivity*

I. Introduction

Among the orthoferrites, lanthanum iron oxide ($LaFeO_3$, LFO) is of great significance for its various technological applications and it has been explored intensively in recent decades [1]. Such a system can be used for a variety of applications, such as detection of humidity, electrode material, sensor material, oxidation catalyst and as an oxygen carrier [2,3]. Modified $LaFeO_3$ with strontium, lanthanum strontium iron oxide (LSF), is also very attractive and it has a perovskite structure with general chemical formula of ABO_3, where A is a large metal ion, typically rare earth or an alkaline earth metal, and B is a small cation, typically a transition metal. Furthermore, LSF can be stable in a reducing atmosphere and it has good electrocatalytic properties for the reduction of oxygen. Therefore doped LFO systems are regularly considered as candidates for chemical looping applications, such as CO_2 splitting, partial oxidation of hydrocarbons or syngas production. At elevated temperature and in reducing conditions lanthanum orthoferrites LFO have been shown to maintain their crystal structure while gradually losing oxygen to form stable $LFO_{3-\delta}$ material, containing iron cations with oxygen non-stoichiometry and mixed valences [4]. For chemical looping applications the main incentive in solid carrier selection will be its cost, inseparably linked to material's stability and abundance. One of the perovskite type compounds that may fulfil these requirements is lanthanum strontium calcium iron oxide LSCF as it does not contain expensive elements or toxic metals. Since the introduction of many novel technologies is strongly dependent on the powder synthesis procedure, considerable effort has been focused on the preparation of lanthanum ferrites and optimization of the experimental conditions [5,6]. Despite these various characteristics, some commercial applications are still limited for $LaFeO_3$. For this reason, many attempts have been made to enhance its performances [7].

When $LaFeO_3$ is doped with Sr or Ca, it shows surprisingly good conductivity, which can be used as conducting ceramic material [8,9]. In the $Ln_{1-x}A_xFeO_3$ (Ln = lanthanides, A = alkali earth) perovskites, Ca is another effective doping-element at the A-site of ABO_3 structure in addition to its low cost [10]. Moreover, Ca could be a good candidate because of the similarity of its ionic radius to La^{3+} which could give rise to higher stability than that in only strontium substituted phases [11]. However, the electrical conductivity

*Corresponding authors: tel: + 48 12 617 24 64,
e-mail: *ppasierb@agh.edu.pl*

of the calcium-doped lanthanum ferrite ($La_{1-x}Ca_xFeO_3$) is less than 90 S/cm (at 550 °C) which is not enough for a proper ionic conductor [12].

Among the adopted approaches, substitution of lanthanum cation with both strontium and calcium ions seems to be compelling. Incorporation of strontium and calcium ions into LFO lattice, i.e. partial substitution of La^{3+} by Sr^{2+} and/or Ca^{2+}, should be compensated by the generation of oxygen vacancies in the perovskite lattice and/or oxidation of a fraction of Fe^{3+} to Fe^{4+} to maintain electroneutrality of the obtained material [13,14].

In the present work, $La_{0.5}Sr_{0.5-x}Ca_xFeO_3$ perovskite-type metal oxides (x = 0.000, 0.025, 0.050, 0.075, 0.100) were prepared by citrate method. The properties of the oxides such as crystal structures and microstructure were characterized by XRD and SEM. In addition, the catalytic reaction activities of the materials were evaluated by temperature-programmed reduction (TPR).

II. Materials and methods

2.1. Sample preparation

For preparing $La_{0.5}Sr_{0.5-x}Ca_xFeO_3$ perovskite (where x = 0.000, 0.025, 0.050, 0.075, 0.100), La_2O_3 (Acros, puriss. p.a., 99.9%), $Sr(NO_3)_2$ (Acros, puriss. p.a., 99+%), CaO (Avantor, puriss. p.a., 99.5%), $Fe(NO_3)_3 \cdot 9\,H_2O$ (Avantor, puriss. p.a., 99.0%), citric acid monohydrate (Avantor, puriss. p.a., 99.0%) and nitric acid (Avantor, puriss. p.a., 65.0%) were used as starting materials. All reagents were analytical grade chemicals and used without further purification. During synthesis, stoichiometric volumes of metal nitrates and oxides according to the atomic ratio of La, Sr, Ca and Fe in $La_{0.5}Sr_{0.5-x}Ca_xFeO_3$ were dissolved in 2 M solution of nitric acid. After mixing, citric acid monohydrate was added. The final concentration ratio of all ions (La, Sr, Ca, Fe) to citric acid was 1:2. The resultant solution was then stirred vigorously for 30 min. Next, the obtained sol was allowed to gel and dry in air at 60 °C overnight and finally heated up to 200 °C for 2 h. The prepared samples were calcined in a muffle furnace from ambient temperature to 850 °C at a rate of 1 °C/min and held for 3 h. The calcination temperature was determined based on TGA-DTA measurements as shown further in the manuscript. The obtained powders were sieved (90 μm), formed into cylindrical pellets and isostatically pressed at 250 MPa. Finally, the samples were sintered at 1200 °C with a heating rate of 10 °C/min.

2.2. Characterization

Laser particle size analyser using dynamic light scattering (DLS) principle was used for measuring particle sizes in the 0.02 to 2000 μm range. For the measurements a blue (488.0 μm wavelength LED) and red (633.8 μm wavelength He-Ne laser) light dual-wavelength, single-lens detection system was used.

Thermogravimetric analysis was used to determine the calcination temperature of the synthesized $La_{0.5}Sr_{0.5-x}Ca_xFeO_3$ samples. Moreover, this method was also applied to analyse the undoped and calcium-doped lanthanum strontium iron oxide samples after the chemical stability tests. The measurements were carried out with the sample mass of 50 mg using a heating rate of 10 °C/min in the flow of synthetic air. The used SDT2960 TA Instruments apparatus is coupled with the mass spectrometer QMD 300 ThermoStar Balzers in order to analyse gases that arise during TGA analysis.

The structural properties of the synthesized samples were analysed by X-ray diffraction (XRD). The phase compositions and lattice parameters were identified by X-ray diffraction analysis, based on the ICDD and ICSD databases. XRD measurements were taken using an Empyrean system (Malvern Panalytical) with monochromatic $CuK_{\alpha 1}$ radiation. The Rietveld refinement method using High Score Plus program was used for calculating the quantitative phase composition and lattice parameters.

Macro- and microstructures of the calcium-doped lanthanum strontium iron oxide were examined using scanning electron microscope (NOVA NANO SEM 200, FEI) equipped with an EDS analyser (EDAX).

Temperature-programmed reduction (TPR) experiments were performed with a thermal conductivity detector in a Gas Sorption System Autosorb iQ Quantachrome. The feed gas was a mixture of 5% H_2/N_2. The temperature was increased from room temperature to 800 °C where it was held for 30 min.

Electrical conductivity was measured using the four-probe method and DC current, under steady-state conditions (temperature gradient less than 5 K) in the temperature range from ambient temperature to 1000 °C.

III. Results and discussion

3.1. Structural characterization

The thermal analyses (TG-DTA) results of the sample $La_{0.5}Sr_{0.5}FeO_3$ are presented in Fig. 1. The initial mass loss below 200 °C is connected with the release of adsorbed water. Next, in the temperature range 300–550 °C, the decomposition and/or combustion of the formed gel can be observed. Finally, decomposition of carbonates leading to perovskite structure formation starts to occur at around 600 °C and ends at around 830 °C. Based on the above results, 850 °C was chosen as a suitable calcination temperature.

XRD analysis (Fig, 2) supports the thesis that 850 °Cwas the proper temperature for calcination as in all $La_{0.5}Sr_{0.5-x}Ca_xFeO_3$ powders only perovskite type structure was observed. It can also be seen that all samples exhibit hexagonal unit cell ($R\bar{3}c$) despite the increasing amount of calcium being substituted for strontium. Additionally, X-ray peaks are slightly shifted toward higher diffraction angles with increasing calcium amount. This indicates that calcium is incorporated in

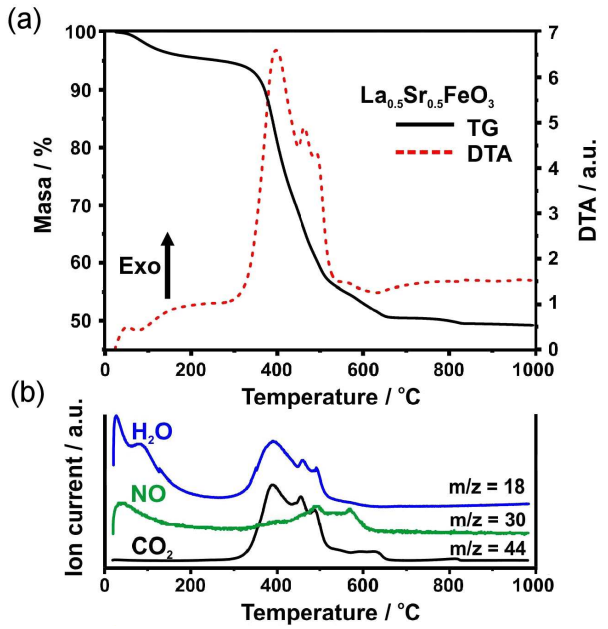

Figure 1. TG and DTA curves for decomposition of $La_{0.5}Sr_{0.5}FeO_3$ precursor (a), M/z = 18, 30 and 44 ion current lines for decomposition of $LaFeO_3$ (b)

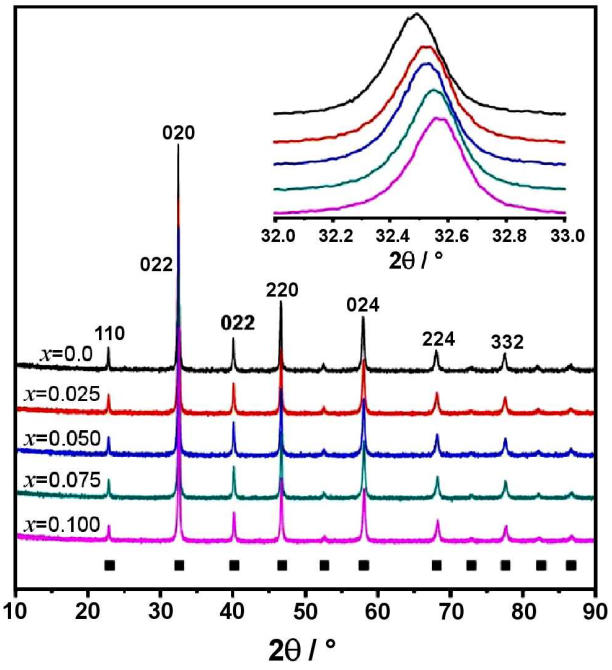

Figure 2. X-ray diffraction pattern of $La_{0.5}Sr_{0.5-x}Ca_xFeO_3$ samples after calcination

Table 1. Unit cell parameters of $La_{0.5}Sr_{0.5-x}Ca_xFeO_3$ samples

Sample	a [Å]	c [Å]	Volume [Å^3]
$La_{0.5}Sr_{0.5}FeO_3$	5.510	13.458	353.84
$La_{0.5}Sr_{0.475}Ca_{0.025}FeO_3$	5.505	13.452	353.04
$La_{0.5}Sr_{0.450}Ca_{0.050}FeO_3$	5.502	13.446	352.50
$La_{0.5}Sr_{0.425}Ca_{0.075}FeO_3$	5.500	13.440	352.09
$La_{0.5}Sr_{0.400}Ca_{0.100}FeO_3$	5.498	13.435	351.70

the lattice since it has smaller ionic radius ($r_{Ca^{2+}}$ = 1.34 Å) than that of Sr^{2+} ($r_{Sr^{2+}}$ = 1.44 Å) [15]. The values of all cell parameters calculated by Rietveld method and abundance of each unit cell type are listed in Table 1. It can be observed that with the increase of calcium substitution both a and c parameters of hexagonal cell decrease.

The microphotographs and particle size distribution diagrams of the powder samples obtained after calcination at 850 °C are presented in Fig. 3. It can be noticed that with an increase in calcium substitution larger agglomerates with denser structure are formed. This can serve as an indicator of a decrease of porosity inside agglomerates. Such behaviour should result in better formation properties leading to the production of denser pellets even before sintering.

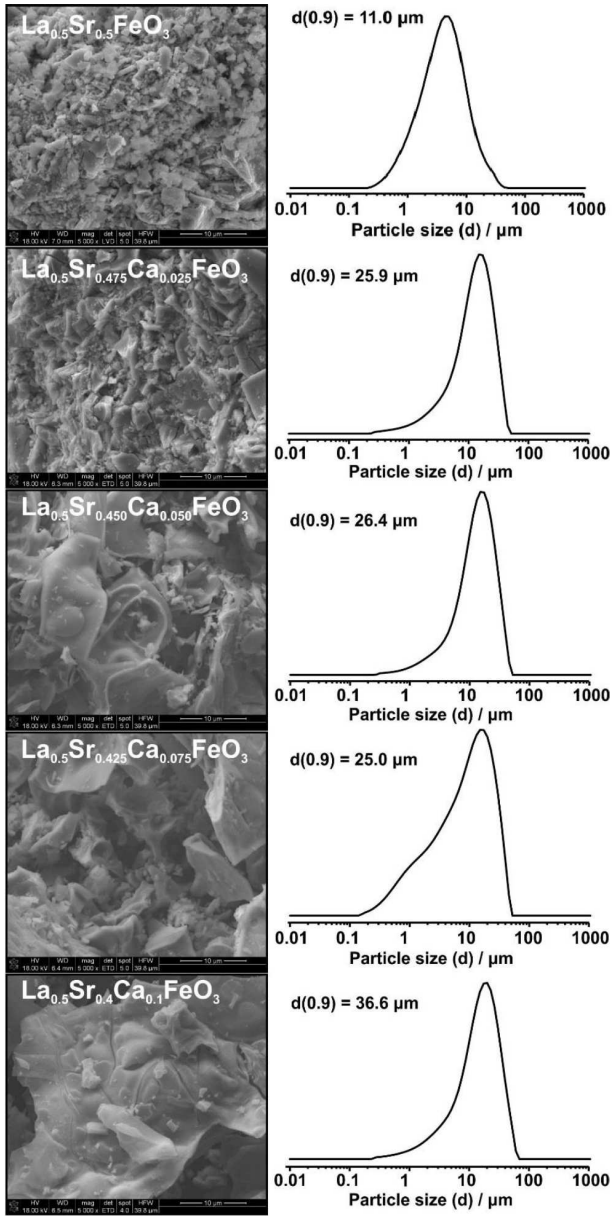

Figure 3. The SEM microphotographs of $La_{0.5}Sr_{0.5-x}Ca_xFeO_3$ powder samples and particle size distribution charts obtained from DLS

Table 2. Porosity, absorbability and apparent density of obtained pellets after sintering at 1200 °C

Sample	Open porosity [%]	Absorbability [%]	Apparent density [g/cm^3]
$La_{0.5}Sr_{0.5}FeO_3$	12.285	2.395	5.107
$La_{0.5}Sr_{0.475}Ca_{0.025}FeO_3$	2.754	0.507	5.405
$La_{0.5}Sr_{0.450}Ca_{0.050}FeO_3$	0.588	0.103	5.570
$La_{0.5}Sr_{0.425}Ca_{0.075}FeO_3$	0.275	0.049	5.654
$La_{0.5}Sr_{0.400}Ca_{0.100}FeO_3$	0.000	0.000	5.693

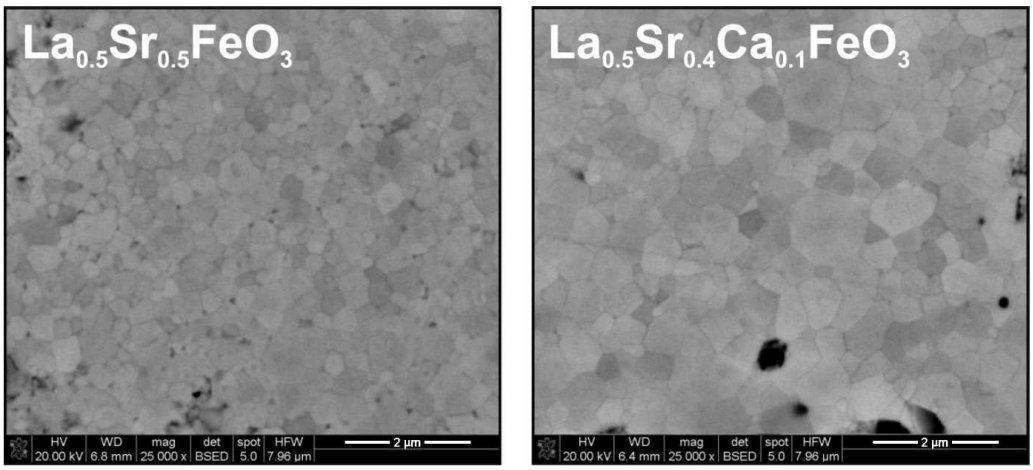

Figure 4. The SEM microphotographs of sintered samples: a) $La_{0.5}Sr_{0.5}FeO_3$ and b) $La_{0.5}Sr_{0.4}Ca_{0.1}FeO_3$

The obtained powders were formed into cylindrical pellets and isostatically pressed at 250 MPa. The pressed pellets were sintered at 1200 °C with a heating rate of 10 °C/min. The temperature was based on our previous studies [16]. Open porosity, absorbability and apparent density of the sintered pellets are given in Table 2. It can be seen that Ca addition has strong influence on sintering. Thus, porosity decreases whereas apparent density increases with the amount of added calcium.

Sintering behaviour of the fabricated samples was investigated by scanning electron microscopy. SEM microphotographs of the undoped sample and the sample with the highest Ca addition, sintered at 1200 °C, are presented in Fig. 4. SEM results reveal uniform grain size distribution and a homogeneous microstructure for the obtained ceramics. Neither significant morphological changes nor segregation phenomenon was detected in SEM micrographs of the substituted samples. However, an increase of the grain size is clearly seen for the sample $La_{0.5}Sr_{0.4}Ca_{0.1}FeO_3$. The average grain sizes were calculated from SEM micrographs and are presented in Table 3. It is obvious that the average grain size increases with the increase of Ca content. Accordingly, Ca^{2+} substitution may be used as a method to control the grain growth and the microstructure homogeneity which can affect the lanthanum strontium ferrite properties. Moreover, it was clearly shown that the host bulk of $La_{0.5}Sr_{0.5}FeO_3$ easily accommodates calcium ions and the hexagonal perovskite structure is preserved.

The grain growth increase could be attributed to the decrease of nucleation sites resulting from higher stacking fault energy due to the calcium incorporation into the perovskite lattice [17].

Table 3. The average grain size of obtained samples after sintering at 1200 °C

Sample	Average grain size [nm]
$La_{0.5}Sr_{0.5}FeO_3$	399
$La_{0.5}Sr_{0.475}Ca_{0.025}FeO_3$	425
$La_{0.5}Sr_{0.450}Ca_{0.050}FeO_3$	430
$La_{0.5}Sr_{0.425}Ca_{0.075}FeO_3$	478
$La_{0.5}Sr_{0.400}Ca_{0.100}FeO_3$	590

3.2. Electrical properties

Electrical properties of the prepared ceramics were tested using the DC method in Ar atmosphere as a function of temperature (RT–1000 °C). Prior to each measurement the sample was equilibrated for 24 h until the reproducible results were obtained. Figure 5a shows the dependence of electrical conductivity as a function of temperature. The electrical conductivity increases with temperature, which is standard behaviour of this type of materials. It can also be observed that conductivity increases with Ca content (except for the sample with x = 0.025). Figure 5b shows the dependence of electrical conductivity as a function of temperature in Arrhenius coordinates. The obtained data allowed to determine the activation energy (E_a), according to the formula:

$$\sigma = A \cdot \exp\left(-\frac{E_a}{2 \cdot T \cdot k_B}\right) \tag{1}$$

where σ is electrical conductivity, T is temperature and k_B is Boltzmann constant. The calculated activation energy in function of Ca content for the sintered samples is presented in Fig. 6b.

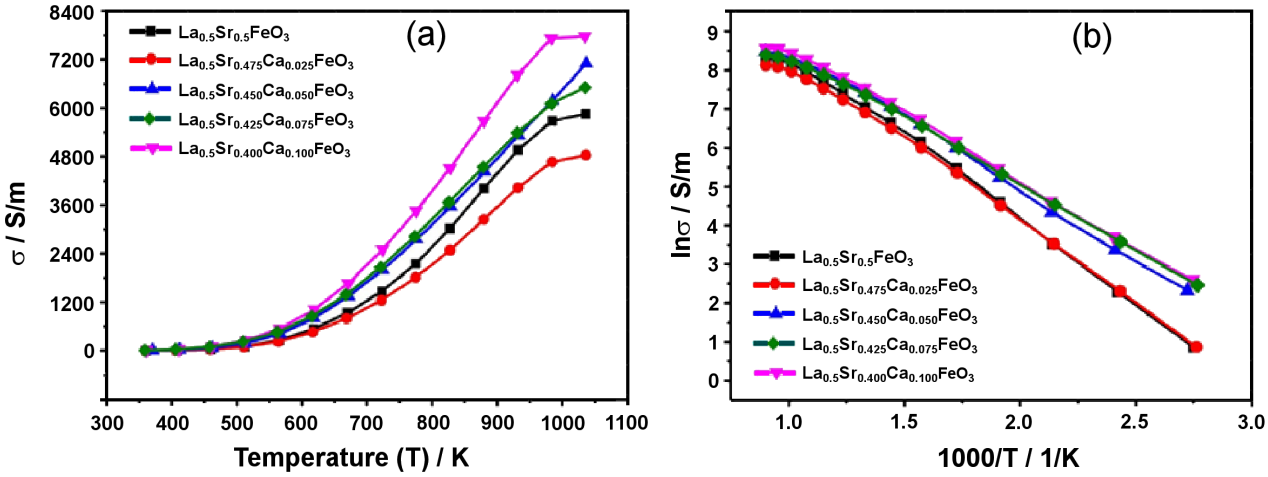

Figure 5. The electrical conductivity of calcium-doped LSF as a function of temperature (a), and in Arrhenius coordinates (b)

The observed dependence of electrical conductivity (Fig. 6d) and activation energy (Fig. 6b) on Ca concentration cannot be explained directly. The possible explanation should take into account the influence of Ca on structure, microstructure and transport properties (diffusivity of ions and electron conduction mechanism). Although the apparent correlations can be proposed for any combination of both structural and electrical parameters the presented results are not sufficient to unequivocally propose the predominant mechanism. According to the conduction mechanism model, it is expected that the decrease of lattice volume should lead to a decrease of electrical conductivity, especially the ionic part. Surprisingly, the decrease of lattice volume with the increase of Ca concentration led to the increase of electrical conductivity. Thus, the influence of microstructure modification may be taken into account. Namely, the increase of average grain size with Ca content may

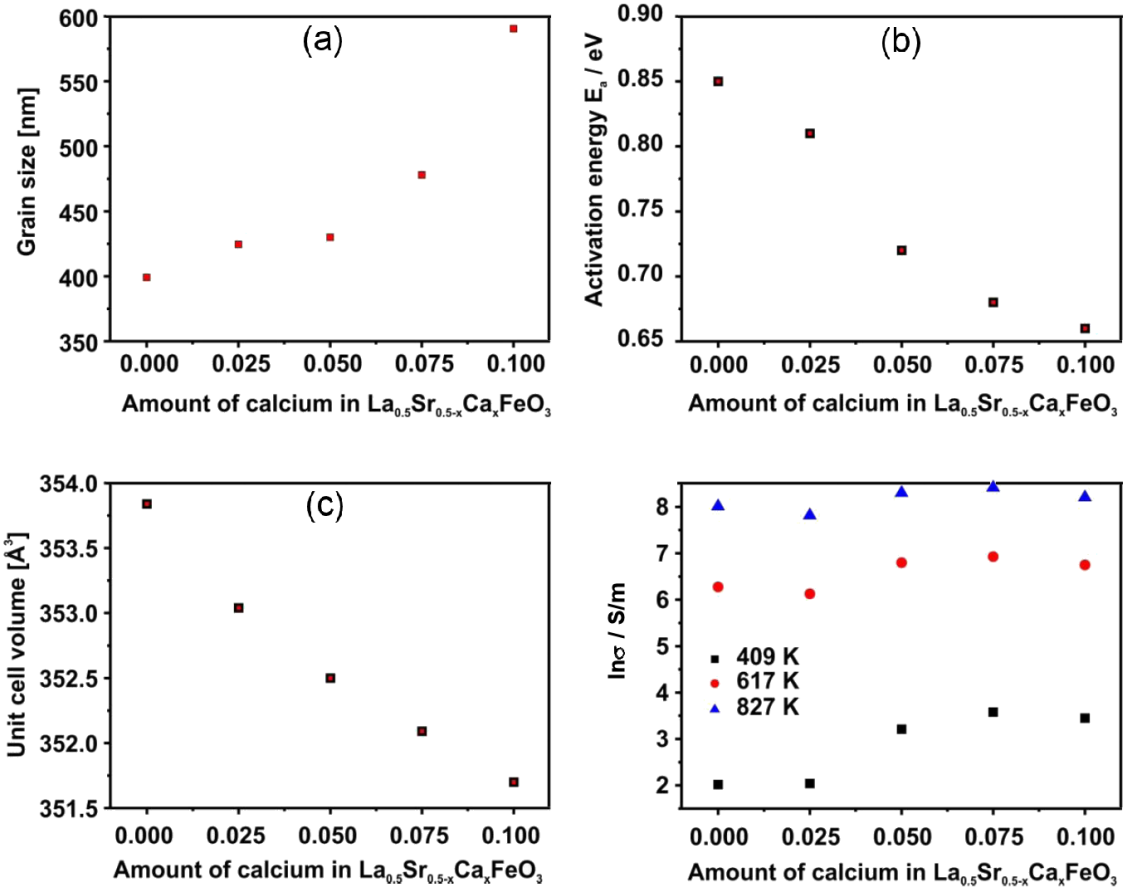

Figure 6. Impact of calcium addition on: a) grain size, b) activation energy, c) unit cell volume and d) lnσ respectively for samples sintered at 1200 °C

be responsible for the increase of electrical conductivity due to the reduction of grain boundaries influence on total electrical conductivity. Taking into account that bulk conductivity is mostly higher than that of grain boundaries, due to the segregation of impurities [18] such hypothesis seems to be plausible. Also, the changes of activation energy with Ca content may be explained in this way; the determined E_a may be treated as apparent activation energy originating from the superposition of bulk and grain boundaries electrical conductivities. The confirmation of the influence of microstructure changes on the dependence of electrical properties on Ca dopant concentration is often possible using the Electrochemical impedance spectroscopy (EIS) measurements. Performed EIS measurements (not presented) have not allowed us the distinction of bulk and grain boundaries effect in EIS spectra, as only one semicircle in Nyquist plot was observed, probably due to the relatively high electrical conductivity of the bulk. The increase of grain size with Ca content, which suggests the increase of ionic diffusivity, correlates well with the conclusions from TPR measurements (TPR results). Thus the evolution of electrical properties with Ca content (as presented in Figs. 5, 6b and 6d) may be also explained in terms of the change of the ionic part in total electrical conductivity.

3.3. Temperature-programmed reduction profiles

The temperature-programmed reduction profiles shown in Fig. 7 demonstrated the reducibility of the samples as a function of temperature and calcium substitution. The first and the second temperature region (separated with dashed line) were evident for each profile. The low-temperature region is related to the formation of additional oxygen vacancies in the $La_{0.5}Sr_{0.5-x}Ca_xFeO_3$ structure.

One can conclude that the higher calcium substitution leads to a high initial concentration of oxygen vacancies in the as-synthesized samples. Due to the Sr^{2+} and Ca^{2+} substitution in the $La_{0.5}Sr_{0.5-x}Ca_xFeO_3$ system, iron coexisted as Fe^{3+} and Fe^{4+}. In the perovskite-type oxides, there are two kinds of oxygen species, called α and β, and both of them are participating in the oxidation reaction of hydrogen. Typically, α oxygen is the non-stoichiometric oxygen, described by oxygen adsorbed on the oxygen deficiency and the excess oxygen, whereas, the β oxygen is associated with the lattice oxygen of B-site cations with high oxidative state or with oxygen species occupying inner vacancies. The second reduction peak is associated with the reduction of B site ions to lower valences, in this case, reduction of the Fe^{4+} and Fe^{3+} to Fe^{2+} or metallic iron. The presence of the second peak and its onset temperature can be assumed as a qualitative description of catalyst reducibility and oxygen mobility within the oxide. Both of those parameters are crucial to describe the catalytic activity and reactivity of the oxides. Note that the amount of an oxygen increases with x, suggesting that Ca^{2+} substitution can enhance the amount of adsorbed oxygen in the $La_{0.5}Sr_{0.5-x}Ca_xFeO_3$ perovskite-type oxides. However, shifts of the two peaks to higher temperatures mean that the activity of the oxygen is slightly decreased with Ca amount increasing [19]. The sample without Ca ($x = 0$) had the lowest onset reduction temperature, whereas Ca substituted samples had the onset temperatures higher up to 250 °C for $La_{0.5}Sr_{0.4}Ca_{0.1}FeO_3$. In these samples, calcium incorporation into the structure increases the phase stability of the oxide. As Ca^{2+} substitution increases, the perovskite-oxides possess an oxygen deficient stable structure at room temperature [20], and the formation capacity of new oxygen vacancies is higher than for a $La_{0.5}Sr_{0.5}FeO_3$ perovskite. Consequently, the calcium-substituted oxides have more formation capabilities for new oxygen vacancies than only Sr^{2+} substituted samples.

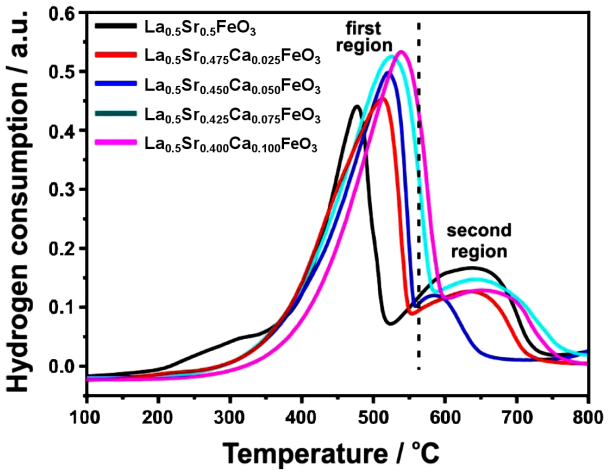

Figure 7. TPR profiles of $La_{0.5}Sr_{0.5-x}Ca_xFeO_3$ samples

IV. Conclusions

In this work, the synthesis and characterization of lanthanum iron oxide compounds were performed. Through the obtained results, it was shown that the citrate method is a simple and convenient route for the preparation of single phase $La_{0.5}Sr_{0.5-x}Ca_xFeO_3$ perovskite (where x varies from 0 to 0.1). From the structural point of view, the hexagonal symmetry was preserved for all the studied compositions. The sintered ceramics have homogeneous microstructure and uniform grain size distribution with the average size which increases with calcium amounts. Conductivity experiments revealed that Ca^{2+} substitution cation may generate the high charge carrier and oxygen vacancy, resulting in the advanced performance of $La_{0.5}Sr_{0.5-x}Ca_xFeO_3$. Initial temperature-programmed studies determined that the highest amount of calcium had the highest structure stability in the reducing environment.

Acknowledgement: Authors are grateful for financial support of the Polish Ministry of Science and Higher

Education within the framework of subvention for science in 2019.

References

1. Z.L. Wang, Z.C. Kang, *Functional and Smart Materials*, Second ed. Plenum Press, New York, 1998.
2. A. Berenov, E. Angeles, J. Rossiny, E. Raj, J. Kilner, A. Atkinson, "Structure and transport in rare earth ferrates", *Solid State Ionics*, **179** (2008) 1090–1093.
3. S. Petrovic, A. Terlecki, L. Karanovic, P. Kirilov-Stefanov, M. Zduji, V. Dondur, D. Paneva, I. Mitov, V. Rakic, "$LaMO_3$ (M = Mg, Ti, Fe) perovskite type oxides: preparation, characterization and catalytic properties in methane deep oxidation", *Appl. Catal. B Environ.*, **79** (2008) 186–198.
4. J. Vieten, B. Bulfin, F. Call, M. Lange, M. Schmücker, A. Francke, M. Roeb, C. Sattler, "Perovskite oxides for application in thermochemical air separation and oxygen storage", *J. Mater. Chem. A*, **4** (2016) 13652–13659.
5. T. Liu, Y. Xu, "Synthesis of nanocrystalline $LaFeO_3$ powders via glucose sol-gel route", *Mater. Chem. Phys.*, **129** (2011) 1047–1050.
6. F. Li, Y. Liu, Z. Sun, R. Liu, C. Kou, Y. Zha, D. Zhao, "Facile preparation of porous $LaFeO_3$ nanomaterial by self-combustion of ionic liquids", *Mater. Lett.*, **65** (2011) 406–408.
7. E. Marek, W. Hu, M. Gaultois, C.P. Grey, S.A. Scott, "The use of strontium ferrite in chemical looping systems", *Appl. Energy*, **223** (2018) 369–382.
8. S.P. Simner, M.D. Anderson, L.R. Pederson, J.W. Stevenson, "Performance variability of $La(Sr)FeO_3$ SOFC cathode with Pt, Ag, and Au current collectors", *J. Electrochem. Soc.*, **152** (2005) 1851–1859.
9. D. Kuscer, M. Hrovat, J. Holc, S. Bernik, D. Kolar, "Some characteristics of Al_2O_3- and CaO-modified $LaFeO_3$-based cathode materials for solid oxide fuel cells", *J. Power Sources*, **61** (1996) 161–165.
10. H.-R. Rim, S.-G. Jeung, E. Jung, J.-S. Lee, "Characteristics of $Pr_{1-x}M_xMnO_3$ (M = Ca, Sr) as cathode material in solid oxide fuel cells", *Mater. Chem. Phys.*, **52** (1998) 54–59.
11. P. Ciambelli, S. Cimino, L. Lisi, M. Faticanti, G. Minelli, I. Pettiti, P. Porta, "La, Ca and Fe oxide perovskites: Preparation, characterization and catalytic properties for methane combustion", *Appl. Catal. B Environ.*, **33** (2001) 193–103.
12. M.S. Hassan, K.B. Shim, O Yang, "Electrocatalytic behavior of calcium doped $LaFeO_3$ as cathode material for solid oxide fuel cell", *J. Nanosci. Nanotechnol.*, **11** (2011) 1429–1433.
13. R. Andoulsi, K. Horchani-Naifer, F. Mokhtar, "Structural and electrical properties of calcium substituted lanthanum ferrite powders", *Powder Technol.*, **230** (2012) 183–187.
14. M. Søgaard, P. Vang-Hendriksen, M. Mogensen, "Oxygen nonstoichiometry and transport properties of strontium substituted lanthanum ferrite", *J. Solid State Chem.*, **180** (2007) 1489–1503.
15. R.D. Shannon, "Revised effective ionic radii and systematic studies of interatomic distances in halides and chaleogenides", *Acta Crystallogr. A Found. Crystallogr.*, **32** (1976) 751–767.
16. Ł. Łańcucki, A. Mizera, A. Łącz, E. Drożdż, M.M. Bućko, P. Pasierb, "Development and chemical stability evaluation of enhanced surface $LaFe_{1-x}Ti_xO_3$ (LFT) perovskites using polystyrene nanospheres as templating agent", *J. Alloys Compd.*, **727** (2017) 863–870.
17. K. Sreejarani, M. Sikhwivhilu, K. Thembela, "Synthesis, characterization and photoluminescence properties of Dy^{3+}-doped nanocrystalline SnO_2", *Mater. Chem. Phys.*, **120** (2010) 619–624.
18. V.V. Kharton, A.L. Shaulo, M. Avdeev, M.V. Patrakeev, F.M.B. Marques, A.P. Viskup, A.A. Yaremchenko, E.N. Naumovich, A.I. Kurbakov, "Perovskite-like system $(Sr,La)(Fe,Ga)O_{3-\delta}$: Structure and ionic transport under oxidizing conditions", *Solid State Ionics*, **150** (2002) 229–243.
19. D. Fino, N. Russo, G. Saracco, V. Specchia, "The role of suprafacial oxygen in some perovskites for the catalytic combustion of soot", *J. Catal.*, **217** (2003) 367–375.
20. T. Nakamura, M. Misono, N. Yoneda, "Catalytic properties of perovskite-type mixed oxides, $La_{1-x}Sr_xCoO_3$", *Bull. Chem. Soc. Jpn.*, **55** (1982) 394–399.